Hydrogels with Differentiated Hydrogen-Bonding Networks for Bioinspired Stress Response

Wei Zhao[a], Baohu Wu[b], Zhouyue Lei*[a] and Peiyi Wu*[a]

[a] Dr. W. Zhao, Dr. Z. Lei, Prof. P. Wu
State Key Laboratory for Modification of Chemical Fibers and Polymer Materials, College of Chemistry and Chemical Engineering
Donghua University
Shanghai 201620, China
E-mail: wupeiyi@dhu.edu.cn; leizhouyue@dhu.edu.cn

[b] Dr. B. Wu
Jülich Centre for Neutron Science (JCNS)
Heinz Maier-Leibnitz Zentrum (MLZ) Forschungszentrum Jülich, Lichtenbergstr
Garching 185748, Germany.

Supporting information for this article is given via a link at the end of the document.

Abstract: Stress response, an intricate and autonomously coordinated reaction in living organisms, holds a reversible, multi-path, and multi-state nature. However, existing stimuli-responsive materials often exhibit single-step and monotonous reactions due to the limited integration of structural components. Inspired by the cooperative interplay of extensor and flexor cells within Mimosa's pulvini, we present a hydrogel with differentiated hydrogen-bonding (H-bonding) networks designed to enable the biological stress response. Weak H-bonding domains resemble flexor cells, confined within a hydrophobic network stabilized by strong H-bonding clusters (acting like extensor cells). Under external force, strong H-bonding clusters are disrupted, facilitating water diffusion from the bottom layer and enabling transient expansion pressure gradient along the thickness direction. Subsequently, water diffuses upward, gradually equalizing the pressure, while weak H-bonding domains undergo cooperative elastic deformation. Consequently, the hydrogel autonomously undergoes a sequence of reversible and pluralistic motion responses, similar to Mimosa's touch-triggered stress response. Intriguingly, it exhibits stress-dependent color shifts under polarized light, highlighting its potential for applications in time-sensitive "double-lock" information encryption systems. This work achieves the coordinated stress response inspired by natural tissues using a simple hydrogel, paving the way for substantial advancements in the development of intelligent soft robots.

Introduction

The stress response is a common phenomenon observed in multicellular organisms, characterized by coordinated interactions among multiple cells and organs, resulting in multi-path and multi-state responses to stimuli.[1] The Mimosa plant can rapidly close its leaflets as a self-protective response to mechanical stimuli, followed by autonomous reopening over time.[2] This dynamic movement is orchestrated by the coordinated regulation of flexor and extensor cells in the Mimosa's pulvini.[3] It operates through an out-of-equilibrium process, enabling living organisms to achieve both essential survival mechanisms and sophisticated functionalities.[4]

However, the response of current artificial materials is often limited to monotonic behavior.[5] When exposed to external stimuli such as light, heat, or chemicals, these materials undergo physical or chemical changes that impact properties such as shape, volume, or chemical composition. Nonetheless, their response behaviors typically rely on a single component, leading to a binary toggling between two states along a linear and monotonic trajectory. The lack of cooperative regulation among multiple structural components restricts the ability of artificial materials to enable the multi-path and multi-state stress response observed in living organisms. Integrating diverse materials[6], employing various stimuli[7], or implementing complex programming steps[8] within a single system can enhance functionality, but the evolution of material properties still depends on individual-specific inputs through equilibrium or quasi-equilibrium processes. Through the digitally controlled photothermal heating, the supramolecular shape-memory polymer enables autonomous off-equilibrium morphing pathways, but it is based on a contrast in the recovery speed (chain relaxation difference induced by temperature gradient) between areas with ink and without ink, with long actuation time (≥10 h).[9] These fundamental disparities contrast with the cooperative modulation from bottom to top observed in nature, which empowers living organisms to exhibit inherent stress response with elevated complexity and reversibility.

Inspired by the underlying mechanism of Mimosa, we propose an approach to design a stress-responsive hydrogel that deviates from conventional hydrogels with the monotonic response. By performing aqueous phase copolymerization with amphiphilic and hydrophobic monomers that form an H-bonding complex, it establishes differentiated H-bonding networks to exhibit the reversible, multi-path, and multi-state stress response observed in living organisms. The amphiphilic monomers facilitate the stabilization of hydrophobic monomers through the formation of hydrogen-bonded complexes. Importantly, these interactions are dynamically adaptable during copolymerization, thus leading to the development of differentiated H-bonding networks. Specifically, the hydrogel's hydrophobic network incorporates strong H-bonding clusters, acting as extensor cells, while the hydrophilic weak H-bonding domains function as flexor cells involved in cooperative elastic deformation. When subjected to

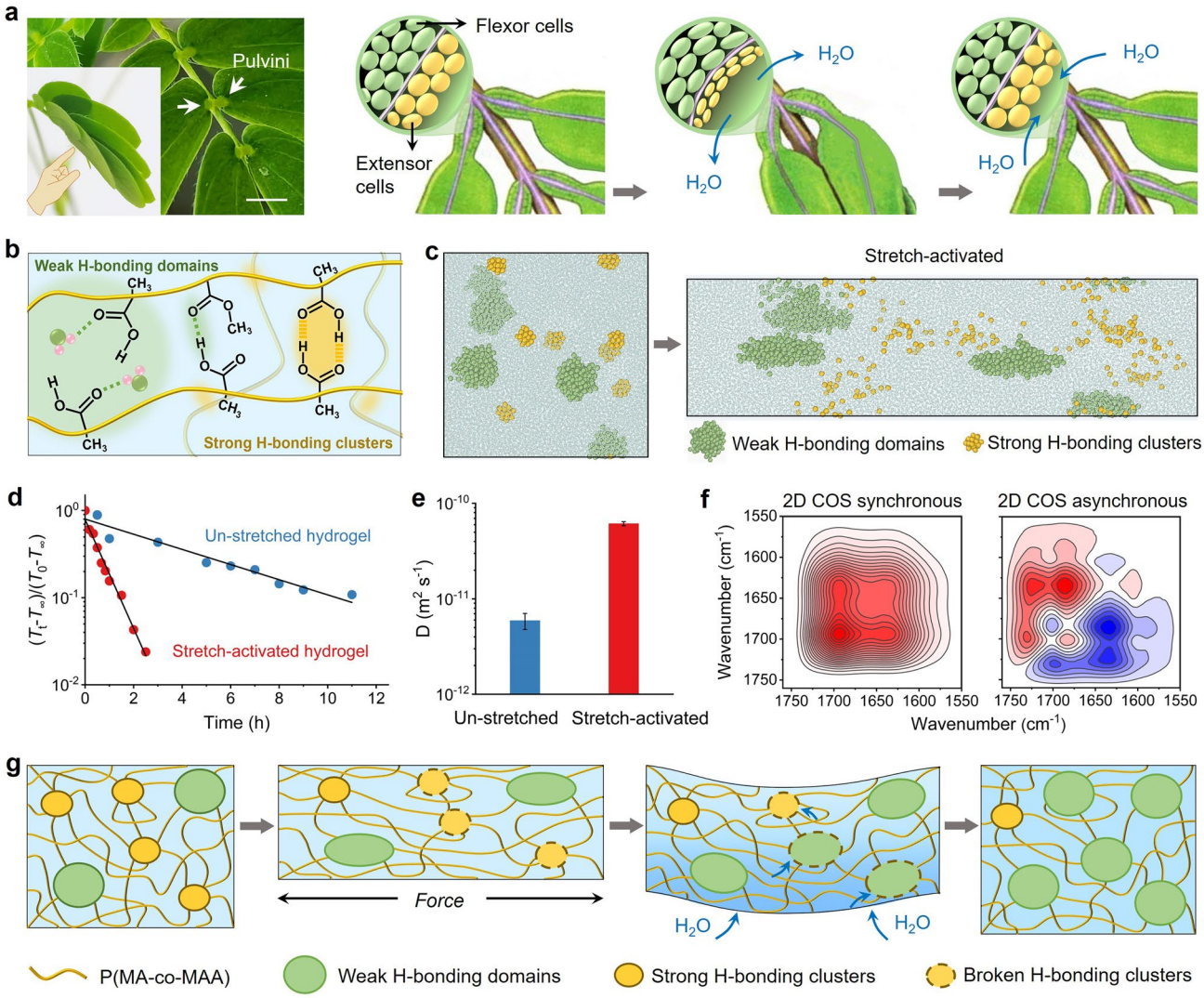

Figure 1. Molecular design and bioinspired mechanism. (a) Photograph of Mimosa's pulvini, and a schematic illustration of the coordinated regulation between their extensor and flexor cells for stress response. Scale bar: 0.2 cm. (b) A schematic illustration of the differentiated H-bonding network structures of the hydrogel. The lines are the P(MA-co-MAA) polymers. The green region is the weak H-bonding domains consisting of PMAA…H_2O and PMA…PMAA, while the yellow region is the strong H-bonding clusters consisting of dimeric PMAA…PMAA. (c) CGMD simulations of changes of the strong H-bonding clusters (yellow) and weak H-bonding domains (green) under the external force. (d) Relative changes of the thickness of the un-stretched and stretch-activated hydrogels during swelling. Black fitting curves are derived from the swelling kinetics equation in Note S6. (e) Cooperative diffusion coefficients (D) of the un-stretched and stretch-activated hydrogels. (f) 2D COS synchronous and asynchronous spectra calculated from Figure S14. In 2D COS spectra, the warm color (red) represents positive intensity, while the cold color (blue) represents negative one. (g) A schematic illustration of the differentiated H-bonding networks of the hydrogel and their cooperative regulation mechanism for the bioinspired stress response.

external forces, the differentiated H-bonding networks are activated, resulting in the hydrogel's autonomous stress response. Furthermore, this process demonstrates remarkable repeatability over multiple cycles and can be programmed to induce pluralistic morphing/locomotion events.

Results and Discussion

Molecular design and bioinspired mechanism

Stress response in Mimosa is controlled by its motor organ, the pulvini, which harmonizes the synchronized volume and shape changes of flexor and extensor cells, resulting in rapid closure and opening of the leaflet (Figure 1a). Upon experiencing mechanical stimuli (e.g., touch), the conformation of aquaporins, which are water channel proteins located on the cell membrane, undergoes changes, leading to the formation of open hydrophilic channels that activate extensor cells.[10] They swiftly release water and thus build a transient expansion pressure gradient. Simultaneously, the flexor cells cooperatively stretch, causing rapid closure of the leaflet. Subsequently, water gradually returns to the extensor cells and distributes uniformly, dissipating the expansion pressure gradient. As a result, the flexor cells relax back to their original state, gradually reopening the leaflet. This cooperative regulation mechanism, functioning through non-equilibrium processes enables Mimosa to exhibit reversible, multi-path, and multi-state stress responses.

Inspired by Mimosa's stress response, we developed a hydrogel with differentiated H-bonding networks. It is prepared through aqueous copolymerization of an H-bonding complex. An amphiphilic monomer, methacrylic acid (MAA), possesses both hydrophobic α-CH_3 and hydrophilic -COOH moieties.[11] This enables the formation of a stable H-bonding complex with a hydrophobic monomer, methyl acrylate (MA), thereby facilitating the homogeneous stabilization of MA in aqueous solutions (Figures S1 and S2). It is noteworthy that the H-bonding complex is dynamically adaptable. As a consequence of the variable strengths of interactions among the two monomers and water, H-bonding between the PMA segments and PMAA segments progressively weakens during the copolymerization, culminating in their gradual metamorphosis into the differentiated H-bonding networks. The Fourier Transform Infrared (FTIR) spectra reveal distinct H-bonding configurations in the P(MA-co-MAA) hydrogel. Notably, the hydrogel is differentiated into strong H-bonding of dimeric PMAA...PMAA at 1694 cm^{-1} and weak H-bonding of PMA…PMAA and PMAA…H_2O at 1718 cm^{-1} (Figure S3). The Low-Field Nuclear Magnetic Resonance (LFNMR) spectra provide evidence that the majority of water exists within the differentiated network in the form of bound water through weak H-bonding (Figure S4 and Note S1).[12] Moreover, the hydrophilic weak H-bonding domains exhibit an average radius of gyration (R_g) of approximately 16 nm, whereas the strong H-bonding clusters have an R_g of about 0.66 nm and are densely distributed within the hydrophobic network, as confirmed by Small-Angle X-ray Scattering (SAXS) spectra (Figure S5 and Note S2). In the resting state, the weak H-bonding domains (acting as flexor cells) are confined within the continuous hydrophobic network, which is stabilized by densely distributed strong H-bonding clusters (acting like extensor cells), as shown in the phase diagrams of atomic force microscope (AFM) (Figure S6) and Figure 1b.

In order to activate the differentiated H-bonding networks, the hydrogel is first softened in 60 °C water. According to the LFNMR and SAXS analysis, the high temperatures (≥60 °C) effectively weaken the strong H-bonding clusters (Figures S7 and S8, Note S3). This allows the hydrogel to be easily stretched to activate the differentiated networks. Afterward, the softened hydrogel is subjected to an external force, and the majority of strong H-bonding clusters are disrupted, leading to cooperative elastic stretching in the weak H-bonding domains. This behavior is elucidated by the LFNMR and SAXS results (Figures S9 and S10). Coarse-grained molecular dynamics (CGMD) simulations indicate that a stretching strain of 150% primarily breaks down the strong H-bonding clusters, while the weak H-bonding domains experience entropic changes in polymer chain elasticity (Figure 1c and Note S4). Notably, an insufficient stretching strain leads to inadequate disruption of strong H-bonding clusters, consequently restricting the activation of the differentiated networks (Figure S11). We further investigate changes in the water content and width of the hydrogel at different times during the activation process (Figure S12 and Note S5). There are minimal changes in both its water content and dimensions. In contrast, the large strain induces disruption of the strong H-bonding clusters is beneficial for water diffusion when the activated hydrogel with differentiated H-bonding networks is immersed in water. Meanwhile, the activated hydrogel switches to an anisotropic elastic state, which also favors water diffusion.[13] Combining the Tanaka-Filmore theory for swelling dynamics and the cooperative diffusion equation, the water diffusion coefficient (D) of the stretch-activated hydrogel is calculated to be 6.2×10^{-11} m^2s^{-1}, significantly higher than that of the resting hydrogel (5.9×10^{-12} m^2s^{-1}, Figure 1d-e, Figure S13, and Note S6).[14]

Subsequently, time-resolved FTIR two-dimensional correlation spectroscopy (2D COS) is employed to track the dynamic changes of the differentiated H-bonding networks during water diffusion (Figure 1f, Figure S14, and Note S7).[14] According to Noda's rule, the response sequence of different chemical groups during water diffusion follows this order: 1686→1697→1606→1635 cm^{-1}, corresponding to ν(COOH) (strong H-bonding clusters), ν(COOH) (weak H-bonding), δ(OH) (PMAA…H_2O), and δ(OH) (H_2O), respectively. This sequence indicates that water molecules initially disrupt the strong H-bonding clusters for swelling and diffusion within the network. However, their impact on the weak H-bonding domains is limited. Additionally, the perturbation-correlation moving window (PCMW) spectrum further demonstrates a significant infiltration of water into the stretch-activated H-bonding network at approximately 265 s, while the weak H-bonding domains remain largely unchanged (Figure S15 and Note S7).[15] The hydrogel at rest shows minimal response to water due to the hindrance of the strong H-bonding clusters (Figure S16). Besides, we also perform comparative analyses with a control sample thoroughly immersed in a sodium thiocyanate solution (known to disrupt hydrophobic interactions).[16] The results show that the hydrogel undergoes negligible disruption of its hydrophobic interactions before and after being stretched (Figure S17). While the peak corresponding to strong hydrogen bonds shows a wavenumber shift (1694→1696 cm^{-1}).

These results confirm that external force activates the differentiated H-bonding networks, enabling water infiltration to swell strong H-bonding clusters and facilitate water diffusion. Meanwhile, the weak H-bonding domains primarily contribute to cooperative elastic deformation. Note that, when the hydrogel is immersed in water, the time difference between the upper and lower surfaces in contact with water is fixed at 2 s. The time delay between the different sides of the hydrogel in contact with the water thus provides the basic conditions for initiating the gradient swelling of the hydrogel. These behaviors are analogous to the coordinated physiological activities of extensor and flexor cells during Mimosa's stress response, providing a basis for the bioinspired stress deformation depicted in Figure 1g.

Bioinspired stress response of the hydrogel

Drawing on the aforementioned molecular design, the hydrogel successfully shows the bioinspired stress response. Initiated by stretching, the hydrogel's differentiated H-bonding networks are activated. Upon contact with water, water molecules rapidly diffuse into the side of the hydrogel that is initially exposed to water, causing it to swell. Subsequently, the opposite side, which comes into contact with water with a 2-second delay, maintains its original state. This creates a transient gradient of water diffusion between the two sides (that is, along the thickness direction of the hydrogel in this case), generating a pressure difference that leads to a slight upward curvature of the hydrogel at 0 seconds under water (Figure 2a). With time passing, the hydrogel undergoes rapid and spontaneous rolling up, followed by a gradual return to its initial flat state, silmilar to Mimosa's stress response upon touch (Figure 2a and Movie S1). In contrast,

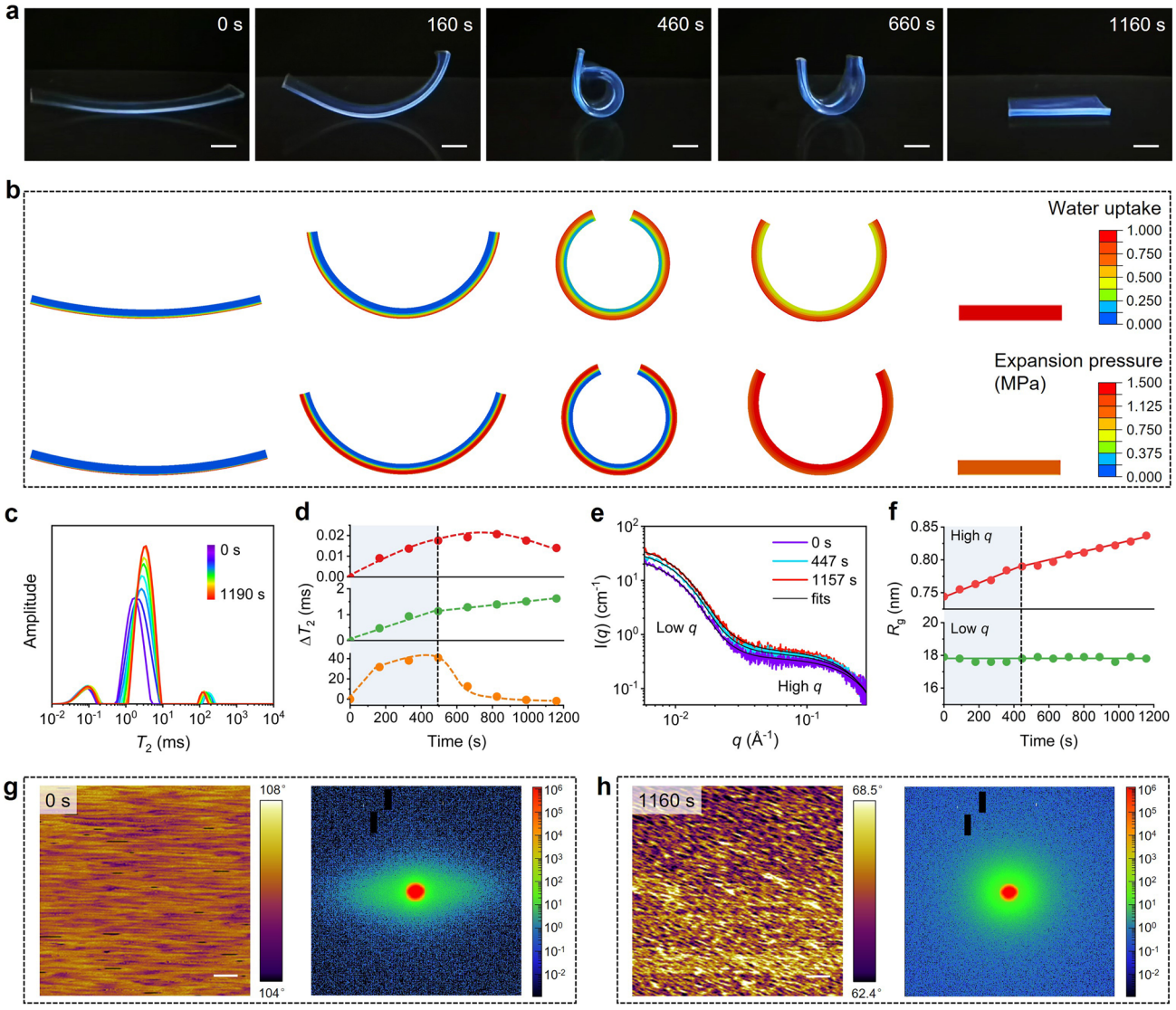

Figure 2. Bioinspired stress response of the hydrogel. (a) The hydrogel that exhibits the stress response similar to that of Mimosa leaf closing and reopening under water. Scale bar: 0.5 cm. (b) Finite element simulations of the changes in water diffusion gradient and expansion pressure gradient during the bioinspired stress response. (c) Time-dependent LFNMR curves of the whole hydrogel during the deformation. (d) Change of the T_2 values (ΔT_2) during the deformation, and ΔT_2=T_2 (t) -T_2 (0 s). The data are derived from Figure 2c. (e) SAXS curves and their fits (black lines) of the whole hydrogel at 0, 447 and 1157 s (the fitting goodness is 1.071, 1.055 and 1.025, respectively) during the morphing event. (f) Change of R_g values of nanostructures during the morphing event. The data are derived from Figure 2e and Figure S23. (g) AFM phase image and corresponding 2D SAXS pattern of the stretch-activated hydrogel before the deformation. The bright regions represent a continuous network stabilized by strong H-bonding clusters, and the dark regions correspond to weak H-bonding domains. Scale bar: 200 nm. (h) AFM phase image and corresponding 2D SAXS pattern of the hydrogel after the deformation under water. Scale bar: 200 nm.

when the hydrogel strip is immersed vertically into water, there is no transient gradient of water diffusion between the upper and lower surfaces. As a result, the activated hydrogel gradually relaxes from its stretched state and returns its original length (Figure S18). On the other hand, as the time difference between the upper and lower surfaces in contact with water increases (e.g., to 4 s), a bigger transient gradient of water diffusion increases the degree of curvature at 0 s underwater (Figure S19). Over time, the hydrogel exhibits a similar process of closing and then reopening, with the time to reach the curled state (360 s) and the total deformation time (1080 s) decreasing (Figure S19). Therefore, the way in which the stretch-activated hydrogel is immersed in water is critical to its bioinspired stress response behavior. Unless otherwise specified, the time difference between the upper and lower surfaces in contact with water is fixed at 2 s. Besides, the large curvatures at the intermediate step can only be achieved when the strong H-bonding is sufficiently disrupted. If the initial activation strain is insufficient (<150%), the hydrogel shows limited angles (Figure S20). This is because the inadequate disruption of strong H-bonding clusters impedes water diffusion, as indicated by the previous CGMD analyses. Finite element simulations reveal that the changes in water diffusion gradient and expansion pressure difference during the stress response (Figure 2b, Note S8, and Table S1). Initially, there is a water distribution and expansion pressure difference within the hydrogel, leading to a closed shape. As time progresses, water diffuses and uniformly distributes within the hydrogel. The expansion pressure difference thus gradually diminishes and eventually disappears, restoring the hydrogel to its initial flat shape. Furthermore, compression can also trigger the stress

response of the hydrogel. However, compared to large-strain stretching (150% strain), small-strain compression (35% strain) results in limited disruption of strong hydrogen bonds. Therefore, while the stress response of the hydrogel triggered by compression exhibits similar response states and paths, the deformation amplitude is smaller (Figure S21). Unless otherwise stated, the conditions for the activation of the differentiated H-bonding networks are chosen to be a stretching strain of 150% and a stretching time of 200 s. Insufficient stress application time (< 200 s) limits the bending angle of the hydrogel, probably due to the insufficient disruption of strong H-bonding clusters. An excessively long stress application time (300 s) results in a slightly delayed response time because the disruption of strong H-bonding clusters has reached saturation (Figure S22). Compared to the Mimosa plant, in which the closing and opening of leaves could be triggered by a simple touch, the hydrogel requires a larger strain to sufficiently disrupt the strong H-bonding clusters and induce significant deformation.

During the stretch-activated stress response process, the dynamic changes of the differentiated H-bonding networks and water distribution are tracked using time-dependent LFNMR spectra (Figure 2c and Note S9). The shortest and longest T_2 values exhibit an initial increase followed by a decrease, whereas the intermediate T_2 value and its peak intensity continuously increase (Figure 2d). These observations indicate that a significant amount of water rapidly infiltrates the hydrophobic network, leading to the swelling of strong H-bonding clusters and the resultant bound water. Subsequently, mobile water diffuses within the network, achieving uniform distribution and generating an increasing number of weak H-bonding domains. To gain more insights into the nano-structure change of the differentiated H-bonding networks, time-resolved SAXS spectra are employed (Figures 2e, S23 and Note S9). In the high q-range, the R_g of the strong H-bonding clusters initially increases rapidly and then gently (Figure 2f). This is a synergistic result of the first massive penetration of water into the strong H-bonding clusters for swelling and the subsequent uniform diffusion in the hydrogel. However, in the low q-range, the R_g remains unchanged, implying that water infiltration has minimal impact on the weak H-bonding domains, which aligns with the findings from the 2D COS spectra. During this process, the weak H-bonding domains primarily undergo cooperative elastic stretching and recovery, akin to the primary function of the flexor cells in Mimosa's pulvinus. Furthermore, AFM phase diagrams and 2D SAXS images visually demonstrate the nano-micro-structure changes in the differentiated H-bonding networks before and after the deforma-

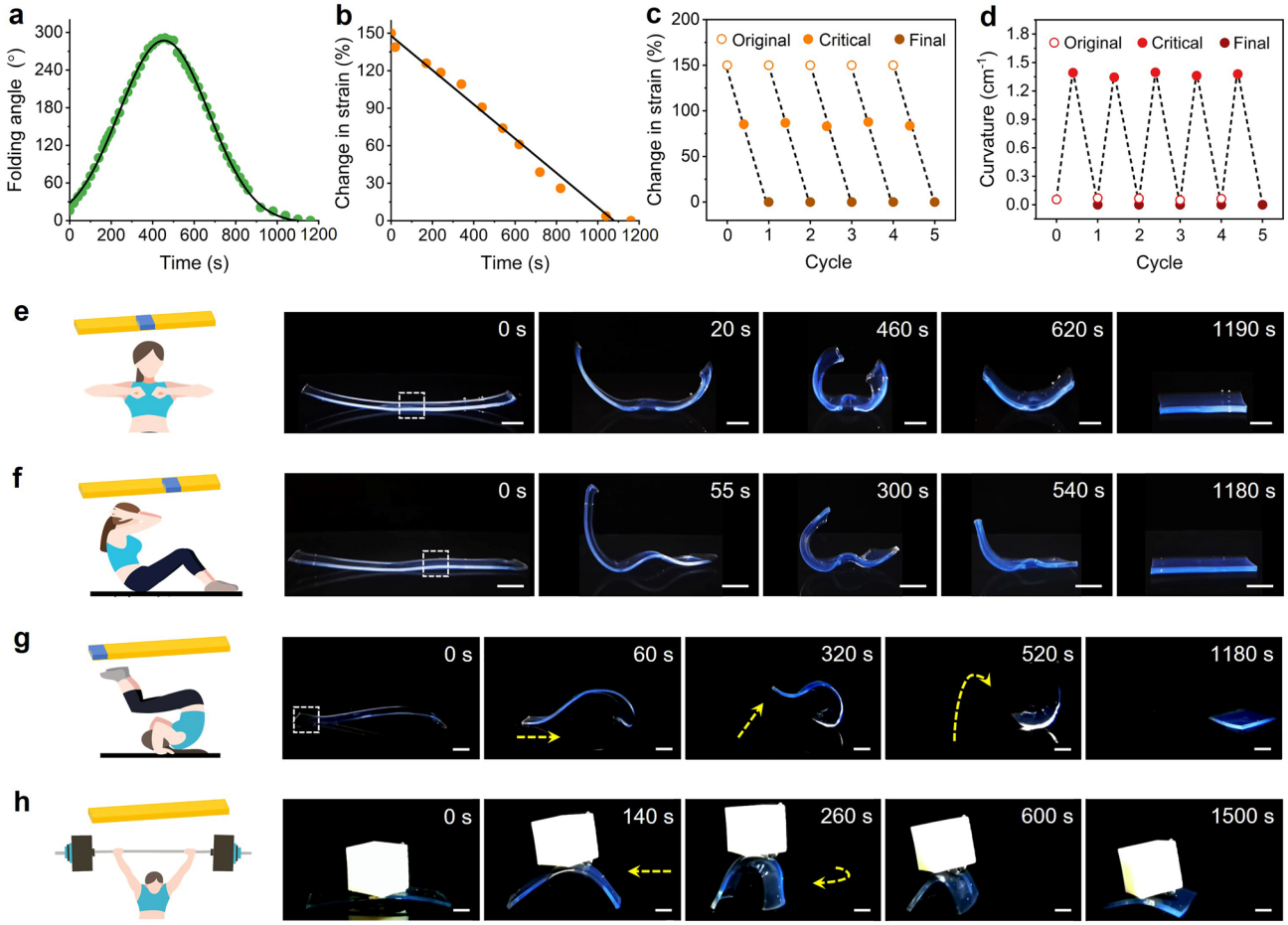

Figure 3. Dynamics of the stress response with reversible, multi-stage, and multi-state features. (a) Time-dependent α during the stress response. (b) Time-dependent $\Delta\varepsilon$ during the stress response. (c) Reversibility of the $\Delta\varepsilon$ in multiple response cycles. (d) Reversibility of the κ in multiple response cycles. (e) The RS and AS module design, a schematic illustration, and photographs of the "expanding" response of the hydrogel under water. The RS module (blue) is the un-stretched region while the AS module (yellow) is the stretch-activated region. The area indicated by the white dashed lines is the RS module. Scale bar: 0.5 cm. (f) The RS and AS module design, a schematic illustration, and photographs of the "sit-up" response of the hydrogel under water. Scale bar: 0.5 cm. (g) The RS and AS module design, a schematic illustration, and photographs of the "forward somersault" locomotion response of the hydrogel under water. Scale bar: 0.5 cm. (h) The AS module design, a schematic illustration, and photographs of the "weightlifting" motion response of the hydrogel under water. Scale bar: 0.5 cm.

tion (Figures 2g and 2h). Upon stretching activation, the weak H-bonding domains extend, aligning the differentiated network (Figure 2g). After the stress response, the weak H-bonding domains recover their initial state with minimal size change (Figure 2h). However, their quantity significantly increases compared to the initial state (Figure S6), attributed to the swelling of strong H-bonding clusters by water molecules. Therefore, the imitation of the stress response in artificial hydrogels could be achieved by a locally to globally cooperative regulation mechanism of the differentiated H-bonding networks.

Dynamics of the stress response and the reversible, multi-stage, and multi-state features

The dynamics of the bioinspired stress response are revealed in Figure 3a-b and Figure S24-25. For the hydrogel with a thickness of 0.6 mm, the folding angle (α) rapidly increases to 291° at about 460 s and gradually returns to 0° at 1160 s (Figure 3a) The change in strain ($\Delta\varepsilon$) linearly decreases over time, from 150 to 0% (Figure 3b). Meanwhile, the curvature (κ), calculated from α and arc length (l), exhibits a similar trend as the α, rapidly increasing and then gradually decreasing to 0 cm^{-1} over time (Figure S25). The hydrogel thus replicates the reversible characteristics observed in Mimosa's stress response. Moreover, the bioinspired stress response of the hydrogel is highly repeatable across multiple cycles, with almost identical $\Delta\varepsilon$, κ, and α (Figure 3c-d and Figure S26). We also investigate the effect of environmental temperature on the response behavior of the hydrogel. As the environment temperature increases, the response speed of the hydrogel accelerates, while the deformation paths and response effects remain stable (Figure S27). Furthermore, the presence of multiple dynamic interactions, particularly the dense and robust H-bonding networks, maintains the resting hydrogel in a glassy state with Young's modulus (E) of approximately 200 MPa (Figure S28). After the cooperative stress response, the differentiated H-bonding network softens due to water infiltration, leading to a decrease in Young's modulus to 12 MPa. However, it can easily return to its initial state by evaporating excess water under ambient conditions. This reversible process mirrors the dynamic interaction with the environment observed during the Mimosa life cycle. Consequently, the reversibility and robustness of the differentiated H-bonding networks empower the hydrogel with long-term stable stress response behavior similar to natural biological systems, surpassing most conventional soft actuators (usually with Young's modulus of less than 10 MPa).[17]

Furthermore, the bioinspired stress response demonstrates multi-path and multi-state characteristics. A triangle hydrogel spontaneously exhibits a series of "bird-like" flapping of wings over time in water (Figure S29). The states of the stress response could be programmed by different distributions of resting-state (RS) modules and active-state (AS) modules in the hydrogel. When the RS module is placed at the center of the elongated AS module, the hydrogel demonstrates a series of "expanding" responses over time (Figure 3e). With the RS module located approximately two-thirds along the elongated AS module, the hydrogel spontaneously performs a sequence of "sit-up" responses (Figure 3f).

More intriguingly, when the RS module is situated at one end of the elongated AS module, the hydrogel executes a series of "forward somersault" response patterns (Figure 3g and Movie S2). This behavior arises from the asymmetric distribution of the RS and AS modules. The AS module initiates an inward arch (closure), propelling the RS module to rapidly shift to the right. Subsequently, significant internal stress is released during the unfolding process, causing the RS module to lift and perform a somersault. Furthermore, within the deformation process, the coordinated changes in the differentiated H-bonding network enable the hydrogel to bear additional weight. Remarkably, the hydrogel adeptly raises a white plastic box by approximately 1.5 cm and gradually lowers it over time ("weightlifting" response, Figure 3h and Movie S3). During deformation, the white plastic box leans to the left, altering the overall center of gravity. Consequently, the hydrogel moves towards the left side and experiences slight rotation. This phenomenon underscores the potential of the hydrogel to dynamically adjust its motion trajectory to accommodate changing weights during deformation. Thus, the editable configuration of the hydrogel itself, along with its RS and AS modules, presents the capacity for diverse sequential deformations and motion responses. This holds significant implications for the development of intelligent soft robots capable of autonomous motion.

In comparison, most existing stimuli-responsive materials exhibit monotonous response behaviors under single environmental stimuli (Note S10 and Table S2). To enhance response complexity, designs often rely on macroscopic heterogeneous structures (such as bilayers and double networks) and leverage environmental changes during the response process to achieve bidirectional deformation.[6c, 8d, 18] However, this inevitably increases the complexity of material fabrication and environment control. In contrast, our hydrogel, based on a single-network macroscopic monolayer structure, demonstrates reversible, multi-path, and multi-state deformation responses in a single water environment. It is simple to prepare and exhibits diverse responses. In addition, the entire deformation time of our hydrogel is short, that is, within 30 minutes (vs. 600-900 minutes for a shape-memory polymer with ample ureidopyrimidinone supramolecular moieties in a previous report[9]).

"Double-lock" information encryption

Upon activation by an external force, the differentiated H-bonding networks of the hydrogel induce birefringence, resulting in vivid colors under polarized light. As the bioinspired deformation progresses, water infiltrates the hydrogel, weakening the differentiated H-bonding networks and enhancing chain mobility and flexibility to gradually release internal stress. The birefringence corresponds to the stress, causing the colors of the hydrogel under polarized light to change over time, revealing a series of morphological and color information.[19] For instance, the hydrogel sequentially exhibits blue "W", brown "W", and white "V" (Figure 4a and Movie S4). Deciphering the blue "W" as true information requires a double unlock. On the one hand, the recognition of the letter "W" is limited to specific periods, with the content during other periods appearing false or blank. On the other hand, the invisible color information requires reading under polarized light. The coupling of time-dependent morphological information with polarized color information facilitates double encryption of the true message, thus enhancing its security. These suggest the diversity and versatility of the encrypted information enabled by the bioinspired hydrogel.

Furthermore, leveraging the influence of water distribution on internal stress allows for spatial control of birefringence color evolution, achieving local information delivery and encryption. As

water evaporates, it enhances the intermolecular interactions within the differentiated H-bonding networks, resulting in denser networks and progressively increasing internal stress.[19b] Consequently, the colors of the hydrogel under polarized light undergo alterations. Here, we utilize silicone oil as an encrypting ink to regulate water evaporation and information delivery (Figure 4b). By covering certain regions of the hydrogel with ink, we arrest water evaporation and induce differential stress distribution between these ink-covered regions and the uncovered ones. Although imperceptible under natural light, this stress pattern leads to varying birefringence colors, enabling time-dependent information delivery and encryption. By directly inscribing "4 7 1" on the stretched hydrogel using ink with a viscosity of 1000 CPS

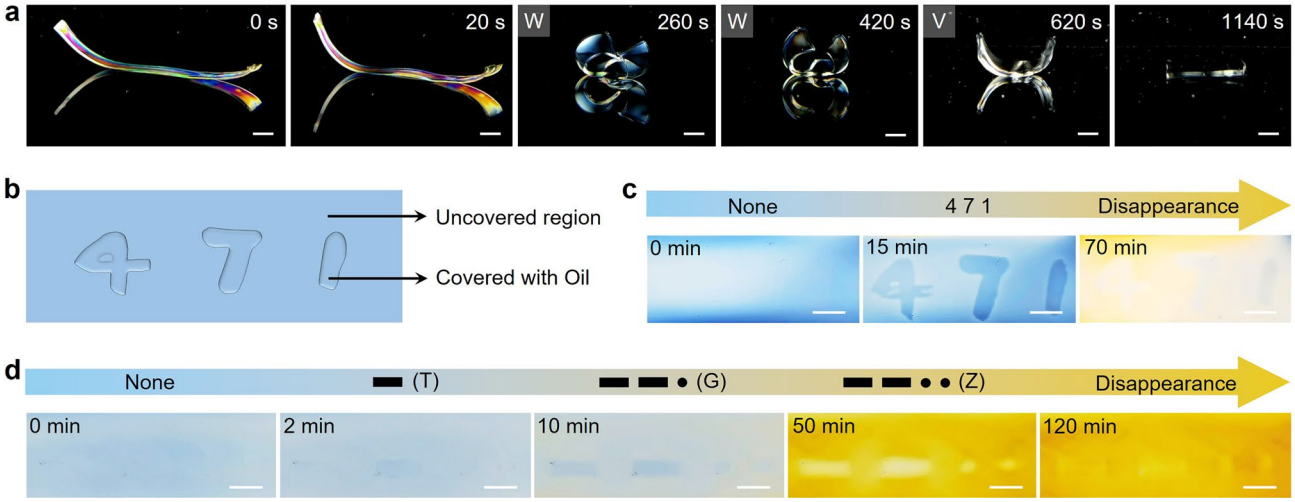

Figure 4. "Double-lock" information encryption. (a) Photographs of time-dependent blue "W", brown "W", and white "V" under polarized light. Scale bar: 0.5 cm. (b) An illustration of how to edit the number patterns that appear over time. (c) The number patterns that appear and disappear over time in polarized light. Scale bar: 0.5 cm. (d) Time-dependent Morse code for information delivery and encryption. Scale bar: 0.5 cm.

(Figure 4c and Movie S5), the numerical information "4 7 1" undergoes a stress-induced evolution, appearing and then disappearing under polarized light. The disappearance occurs when both regions reach equilibrium stress levels, effectively eliminating spatial color differences. Furthermore, using ink with a viscosity of 3500 CPS, we create a series of dolphin patterns in blue, white, and yellow over time, which eventually fade away (Figure S30). Compared to the numerical information evolution in Figure 4c, the appearance of these patterns is faster. This phenomenon can be attributed to the higher ink viscosity, resulting in slower water evaporation and more pronounced spatial color differences between the ink-covered region and the regions with rapid evaporation (uncovered by the ink). This differential evaporation rate contributes to a swifter manifestation of the information.

Therefore, the combination of inks with different viscosities enables more intricate sequential information delivery and encryption. Morse code, composed of simple characters represented by short signals "•" and long signals "—", serves as an effective means of communication. Employing inks with varying viscosities (100, 1000, and 3500 CPS), we inscribe "— — • •" onto the hydrogel (Figure 4d, Figure S31, and Movie S6). The "—" Morse code covered with the ink of 3500 CPS viscosity initially appears at 2 minutes, corresponding to the letter "T". At 10 minutes, in combination with the region covered by the ink of 1000 CPS viscosity, the hydrogel displays the "— — •" code, representing the letter "G". Subsequently, at 50 minutes, the complete information appears, i.e., the "— — • •" code indicating the letter "Z". Since "TZ" is the true information, its decoding requires information retrieval and recording at both 2 minutes and 50 minutes. This time-dependent superposition of encrypted information further amplifies the intricacy of information decryption. Consequently, the water-driven stress changes in the differentiated H-bonding networks cause the hydrogel to display different morphologies, numbers, and texts.

Conclusion

In summary, this work designs a hydrogel with differentiated H-bonding networks to achieve Mimosa-inspired stress response behavior. Compared to the natural mimosa, the stress-responsive hydrogel has some limitations, such as the requirement of programmed stretching and a time delay between the different sides of the hydrogel in contact with the water, but it also follows a cooperative regulation mechanism that allows different deformation/locomotion responses along off-equilibrium pathways. This is different from the actuation mechanism of previous artificial responsive materials through the heterogeneous design of macrostructures (e.g., bilayers, gradient structures, or differences in polymer chain relaxation). External forces disrupt the strong H-bonding clusters, activating the differentiated H-bonding networks. Water infiltrates the strong H-bonding clusters (as extensor cells) unevenly along the thickness direction, then diffuses and redistributes uniformly. Meanwhile, the weak H-bonding domains (as flexor cells) undergo cooperative elastic deformation. The autonomous non-equilibrium response patterns of the hydrogel exhibit high repeatability over multiple cycles and can be programmed. These properties are similar to the reversible, multi-path, and multi-state stress responses observed in living organisms. Furthermore, the hydrogel shows significant potential for a rare time-dependent "double-lock" information encoding system, as evidenced by its remarkable water-driven stress-dependent color change under

polarized light. Unlike conventional stimuli-responsive materials, this hydrogel shed new insights into the design of bioinspired materials with a cooperative regulation mechanism, paving the way for the next generation of intelligent soft robotics.

Acknowledgements

We gratefully acknowledge the financial support from the National Natural Science Foundation of China (No. 22305033 received by Z.L., No. 52161135102 received by P.W.) and the Fundamental Research Funds for the Central Universities (No. 23D210502 received by Z.L.).

Keywords: Hydrogels • hydrogen-bonding networks • stress response • motion response • information encryption

[1] a) H. Zhang, J. Zhu, Z. Gong, J.-K. Zhu, *Nat. Rev. Genet.* **2022**, *23*, 104-119; b) T. Eisner, *PNAS* **1981**, *78*, 402-404; c) J. Braam, *New Phytol.* **2005**, *165*, 373-389.

[2] T. Hagihara, M. Toyota, *Plants* **2020**, *9*, 587.

[3] G. Asprey, J. Palmer, *Nature* **1955**, *175*, 1122-1122.

[4] a) U. G. Wegst, H. Bai, E. Saiz, A. P. Tomsia, R. O. Ritchie, *Nat. Mater.* **2015**, *14*, 23-36; b) A. Walther, *Adv. Mater.* **2020**, *32*, 1905111; c) R. Merindol, A. Walther, *Chem. Soc. Rev.* **2017**, *46*, 5588-5619.

[5] a) Z.-Z. Nie, B. Zuo, M. Wang, S. Huang, X.-M. Chen, Z.-Y. Liu, H. Yang, *Nat. Commun.* **2021**, *12*, 2334; b) B. Jin, J. Liu, Y. Shi, G. Chen, Q. Zhao, S. Yang, *Adv. Mater.* **2021**, *34*, 2107855; c) W. Miao, B. Yang, B. Jin, C. Ni, H. Feng, Y. Xue, N. Zheng, Q. Zhao, Y. Shen, T. Xie, *Angew. Chem. Int. Ed.* **2022**, *134*, e202109941; d) F. Zhang, D. Li, C. Wang, Z. Liu, M. Yang, Z. Cui, J. Yi, M. Wang, Y. Jiang, Z. Lv, S. Wang, H. Gao, X. Chen, *Nat. Commun.* **2022**, *13*, 7294; e) W. Zhao, Z. Lei, P. Wu, *Adv. Sci.* **2023**, *10*, 2300253; f) Z. Lei, W. Xu, G. Zhang, *Smart Med.* **2023**, *2*, e20220026; g) S. Wei, W. Lu, H. Shi, S. Wu, X. Le, G. Yin, Q. Liu, T. Chen, *Adv. Mater.* **2023**, *35*, 2300615; h) Y. Qi, L. Song, C. Zhou, S. Zhang, *Adv. Mater.* **2023**, *35*, 2210753; i) X. Qian, Y. Zhao, Y. Alsaid, X. Wang, M. Hua, T. Galy, H. Gopalakrishna, Y. Yang, J. Cui, N. Liu, M. Marszewski, L. Pilon, H. Jiang, X. He, *Nat. Nanotechnol.* **2019**, *14*, 1048-1055; j) H. Zhang, H. Zeng, A. Priimagi, O. Ikkala, *Nat. Commun.* **2019**, *10*, 3267; k) Z. Lei, P. Wu, *Matter* **2023**, *6*, 429-444; l) T. Zheng, M. Runowski, I. R. Martín, K. Soler-Carracedo, L. Peng, M. Skwierczyńska, M. Sójka, J. Barzowska, S. Mahlik, H. Hemmerich, F. Rivera-López, P. Kulpiński, V. Lavín, D. Alonso, D. Peng, *Adv. Mater.* **2023**, *35*, 2304140; m) Y. Hao, Z. Gong, Z. Xie, S. Guan, X. Yang, T. Wang, L. Wen, *J. Bionic Eng.* **2018**, *15*, 220-235; n) F. Zhao, W. Rong, L. Wang, L. Sun, *J. Bionic Eng.* **2021**, *18*, 799-811.

[6] a) C. Y. Li, D. Jiao, X. P. Hao, W. Hong, Q. Zheng, Z. L. Wu, *Adv. Mater.* **2023**, *35*, 2211802; b) Z. Jiang, B. Diggle, I. C. G. Shackleford, L. A. Connal, *Adv. Mater.* **2019**, *31*, 1904956; c) S. Wu, H. Shi, W. Lu, S. Wei, H. Shang, H. Liu, M. Si, X. Le, G. Yin, P. Theato, T. Chen, *Angew. Chem. Int. Ed.* **2021**, *60*, 21890-21898; d) X. Yang, L. Lan, X. Pan, Q. Di, X. Liu, L. Li, P. Naumov, H. Zhang, *Nat. Commun.* **2023**, *14*, 2287; e) Y. Zhao, Q. Li, Z. Liu, Y. Alsaid, P. Shi, M. Khalid Jawed, X. He, *Sci. Robot* **2023**, *8*, eadf4753.

[7] a) J. Kim, J. A. Hanna, M. Byun, C. D. Santangelo, R. C. Hayward, *Science* **2012**, *335*, 1201-1205; b) M. Liu, L. Jin, S. Yang, Y. Wang, C. B. Murray, S. Yang, *Adv. Mater.* **2023**, *35*, 2208613.

[8] a) Y. Huang, Y. Xu, H. K. Bisoyi, Z. Liu, J. Wang, Y. Tao, T. Yang, S. Huang, H. Yang, Q. Li, *Adv. Mater.* **2023**, *35*, 2304378; b) X. P. Hao, Z. Xu, C. Y. Li, W. Hong, Q. Zheng, Z. L. Wu, *Adv. Mater.* **2020**, *32*, 2000781; c) H. Lu, B. Wu, X. Le, W. Lu, Q. Yang, Q. Liu, J. Zhang, T. Chen, *Adv. Funct. Mater.* **2022**, *32*, 2206912; d) Y. Zhang, K. Liu, T. Liu, C. Ni, D. Chen, J. Guo, C. Liu, J. Zhou, Z. Jia, Q. Zhao, P. Pan, T. Xie, *Nat. Commun.* **2021**, *12*, 6155.

[9] W. Peng, G. Zhang, Q. Zhao, T. Xie, *Adv. Mater.* **2021**, *33*, 2102473.

[10] a) P. Fleurat-Lessard, N. Frangne, M. Maeshima, R. Ratajczak, J. L. Bonnemain, E. Martinoia, *Plant Physiol.* **1997**, *114*, 827-834; b) K. Prado, C. Maurel, *Front. Plant Sci.* **2013**, *4*, 255.

[11] Z. Lei, B. Wu, P. Wu, *Research* **2021**, *2021*, 4515164.

[12] S. Wu, Z. He, J. Zang, S. Jin, Z. Wang, J. Wang, Y. Yao, J. Wang, *Sci. Adv.* **2019**, *5*, eaat9825.

[13] a) W. Hong, X. Zhao, J. Zhou, Z. Suo, *J. Mech. Phys. Solids* **2008**, *56*, 1779-1793; b) W. Hong, Z. Liu, Z. Suo, *Int. J. Solids Struct.* **2009**, *46*, 3282-3289.

[14] a) I. Noda, *Vib. Spectrosc.* **2012**, *60*, 146-153; b) I. Noda, *J. Am. Chem. Soc.* **1989**, *111*, 8116-8118.

[15] S. Morita, H. Shinzawa, I. Noda, Y. Ozaki, *Appl. Spectrosc.* **2006**, *60*, 398-406.

[16] P. H. C. Paiva, Y. L. Coelho, L. H. M. da Silva, M. S. Pinto, M. C. T. Vidigal, A. C. d. S. Pires, *Food Chem.* **2020**, *305*, 125463.

[17] a) Y. Yan, T. Santaniello, L. G. Bettini, C. Minnai, A. Bellacicca, R. Porotti, I. Denti, G. Faraone, M. Merlini, C. Lenardi, P. Milani, *Adv. Mater.* **2017**, *29*, 1606109; b) Y. Cheng, K. H. Chan, X. Q. Wang, T. Ding, T. Li, C. Zhang, W. Lu, Y. Zhou, G. W. Ho, *Adv. Funct. Mater.* **2021**, *31*, 2101825; c) G. Zhu, Y. Hou, N. Xia, X. Wang, C. Zhang, J. Zheng, D. Jin, L. Zhang, *Adv. Funct. Mater.* **2023**, *33*, 2300888.

[18] S. Hu, Y. Fang, C. Liang, M. Turunen, O. Ikkala, H. Zhang, *Nat. Commun.* **2023**, *14*, 3717.

[19] a) G. Zhang, W. Peng, J. Wu, Q. Zhao, T. Xie, *Nat. Commun.* **2018**, *9*, 4002; b) J. Bai, Z. Shi, X. Jiang, *Adv. Funct. Mater.* **2023**, *33*, 2301797.